Article ID: 1000-324X(2016)09-0997-07 **DOI:** 10.15541/jim20160060

Microstructure and Thermoelectric Properties of p-type $Si_{80}Ge_{20}B_{0.6}$-SiC Nanocomposite

YANG Xiao-Yan[1, 3], WU Jie-Hua[2], REN Du-Di[2], ZHANG Tian-Song[2], CHEN Li-Dong[1]

(1. State Key Laboratory of High Performance Ceramics and Superfine Microstructure, Shanghai Institute of Ceramics, Chinese Academy of Sciences, Shanghai 200050, China; 2. CAS Key Laboratory of Materials for Energy Conversion, Shanghai Institute of Ceramics, Chinese Academy of Sciences, Shanghai 200050, China; 3. University of Chinese Academy of Sciences, Beijing 100049, China)

Abstract: P-type silicon germanium (SiGe) alloys, $Si_{80}Ge_{20}B_{0.6}$, with homogeneously dispersed SiC nanoparticles were prepared by ball milling and subsequent spark plasma sintering. The influence of grain size reduction of SiGe matrix and SiC nanoparticle dispersion on electrical and thermal transport properties were investigated. A significant reduction in lattice thermal conductivity is achieved by a more pronounced grain boundary scattering of phonons introduced by grain size reduction after ball milling. Dispersing SiC nanoparticles in the $Si_{80}Ge_{20}B_{0.6}$ matrix effectively reduces the conduction of heat by providing additional phonon scattering centers. A dimensionless figure-of-merit (*ZT*) of 0.62 at 1000 K is obtained in nanostructuring $Si_{80}Ge_{20}B_{0.6}$ incorporated with only 0.5vol% SiC nanoparticles, which is 17% higher than the parent $Si_{80}Ge_{20}B_{0.6}$ matrix and about 30% higher than p-type SiGe alloy used in the radioisotope thermoelectric generator in space missions.

Key words: SiGe alloys; SiC nanoparticle dispersion; thermoelectric material; nanocomposite; nanostructuring

SiGe alloys have been used as thermoelectric materials in radioisotope thermoelectric generators (RTGs) to convert radio-isotope heat into electricity and are also suitable candidates for other high temperature thermoelectric (TE) applications such as waste heat recovery on account of their promising TE properties and excellent reliability at high temperatures[1-3]. The performance of TE materials depends on the dimensionless figure-of-merit $ZT = (\alpha^2\sigma/\kappa)T$, where α is the Seebeck coefficient, σ is the electrical conductivity, κ is the thermal conductivity and T is the absolute temperature. In the past decades, a number of attempts have been made to enhance the TE performance of SiGe alloys and these achievements can be divided into two aspects: the improvements of *ZT* in bulk materials by nanostructuring, nanocomposite and optimized doping; the innovations in low-dimensional materials such as quantum dots, nanowires, superlattices and thin films[4-9]. Especially, the bulk SiGe materials exhibit great advantages in fabrication and practical application. The efforts to enhance the *ZT* values of bulk SiGe alloys through nanostructuring and nanocomposite approaches are kept on going and great achievements have been made.

Nanostructuring approach has been utilized to effectively decrease the thermal conductivity by scattering phonons due to the numerous interfaces introduced by the grain size reduction[10-11]. Chen, *et al* reported remarkable enhancement in *ZT* values in SiGe alloys with nano-grain structure prepared by ball milling. The *ZT* of p-type SiGe alloys was increased from 0.65 to 0.95 at 1073–1173 K while the *ZT* of n-type was improved from 0.93 to 1.3[12-13]. Furthermore, the highest values of *ZT* similar to 1.84 at 1073 K and 1.2 at 1173 K were reported for n-type and p-type nanostructured SiGe alloys, respectively[14-16]. Similar approach was also reported for making nanostructured p-type bulk bismuth antimony telluride with a peak *ZT* of 1.4 at 373 K[17]. Nanocomposite, as another important solution to introduce additional centers and interfaces for phonons scattering, has also been proved effective for enhancing *ZT* in many bulk materials. Zhou, *et al*[18] fabricated skutterudites with dispersed Ag nanoparticles by ball milling and found 30% enhancement in *ZT* value. Zhao and Ding prepared the $Yb_yCo_4Sb_{12}$-based nanocomposite containing well-distributed nano-Yb_2O_3 particles by *in-situ* oxidation process, which effectively scatters phonons but only slightly impacts electron transport and generates a significant *ZT* enhancement[19-20]. In addition, a high *ZT* value of 1.33 at 372 K was obtained in BiSbTe-based composite with dispersion of 0.4vol% SiC

Received date: 2016-01-27; **Modified date:** 2016-03-25
Foundation item: National Natural Science Foundation of China (51372261, 51402337)
Biography: YANG Xiao-Yan(1988–), female, candidate of PhD. E-mail: yangxy116@student.sic.ac.cn
Corresponding author: CHEN Li-Dong, professor. E-mail: cld@mail.sic.ac.cn

nanoparticles[21]. For SiGe alloys, Mingo, *et al* proposed a "nanoparticle-in-alloy" approach to improve the TE properties and performed theoretical calculation. Their calculation results showed that strong reduction in thermal conductivity could be obtained by the dispersion of different types of metal or semiconductor silicide nanoparticles in the SiGe matrix, while the electronic transport properties would not be negatively influenced through optimizing the nanoparticle size[22]. In the matter of experiment, an n-type SiGe-$MoSi_2$ nanocomposite was synthesized by mixing a small amount of molybdenum nanoparticles that react *in-situ* with the SiGe matrix and form $MoSi_2$ nanoparticles (~60 nm) during spark plasma sintering. The maximum *ZT* reached about 1.0 at 973 K in the $MoSi_2$ nanoparticles dispersed SiGe alloy[23].

In this work, we combine nanostructuring (grain size reduction) with nanocomposite (dispersing SiC nanoparticles) approaches to achieve the enhancement of TE performance in SiGe alloys ($Si_{80}Ge_{20}B_{0.6}$). SiC possesses high melting point, excellent chemical stability and therefore is expected to benefit improving the high temperature stability of the nanostructure. At the same time, SiC nanoparticle dispersion would not evidently affect the electronic transport in SiGe-SiC nanocomposite because SiC exhibits semi-conducting behavior. Our systematical study on the influence of grain size reduction of SiGe alloys matrix and nano-SiC second phase on the electrical and thermal transport properties of SiGe-SiC nanocomposite demonstrates that nanostructuring and nanocomposite can be employed simultaneously to enhance TE performance.

1 Experimental

The ingots of $Si_{80}Ge_{20}B_{0.6}$ were firstly prepared by induction melting the elements of 99.999% Si, 99.999% Ge and 99.99% B in the desired stoichiometry at 1673 K, then were further annealed at 1423 K for 72 h. The as-prepared ingots were ground into powder using agate mortar for $Si_{80}Ge_{20}B_{0.6}$ matrix powder, then the grain was further refined by ball milling process (500 r/min, 4 h, Fritsch-Pulverisette-7). To prepare the $Si_{80}Ge_{20}B_{0.6}$-SiC composite powder, SiC nanoparticles with size of about 50 nm were dispersed into the $Si_{80}Ge_{20}B_{0.6}$ matrix using the same ball milling process. Then the $Si_{80}Ge_{20}B_{0.6}$ matrix powder without ball milling process, the ball-milled $Si_{80}Ge_{20}B_{0.6}$ powder and these ball-milled composite powders were consolidated by spark plasma sintering (SPS) at 1323 K for 10 min under an axial pressure of 50 MPa. The samples obtained by the above process are denoted as $Si_{80}Ge_{20}B_{0.6}$ matrix, $Si_{80}Ge_{20}B_{0.6}$ BM and a series of $Si_{80}Ge_{20}B_{0.6}$ + *x*vol% SiC BM (x = 0.3, 0.5, 1.0), respectively.

The phase structure was examined by X-ray diffraction (XRD) using Cu Kα radiation (Rigaku D/max 2550 V). The microstructure was investigated with field emission electron microscope (SEM, ZEISS Supra 55) and transmission electron microscope (TEM, FEI Tecnai G2 F20) equipped with an energy dispersive spectrometer (EDS).

The Hall resistance (R_H) was obtained by a Quantum Design PPMS instrument. The carrier concentration (n) and mobility (μ) were calculated from $n = 1/eR_H$ and $\mu = \sigma R_H$, respectively, where σ is the electrical conductivity and e is the elementary charge. The electrical conductivity (σ) and Seebeck coefficient (α) were measured using the Seebeck coefficient/electrical resistance measuring system (ZEM-3, ULVAC-RIKO). The thermal conductivity (κ) was calculated using the equation $\kappa=\lambda C_p d$, where λ, C_p and d are the thermal diffusivity, heat capacity and density. The thermal diffusivity was obtained by the laser flash method (LFA427, NETZSCH), the heat capacity adopted the values of reference[4], and the density was measured using the Archimedes method.

2 Results and discussion

Fig. 1 shows the powder XRD patterns of crushed $Si_{80}Ge_{20}B_{0.6}$ ingot ($Si_{80}Ge_{20}B_{0.6}$ matrix sample), ball-milled $Si_{80}Ge_{20}B_{0.6}$ ($Si_{80}Ge_{20}B_{0.6}$ BM sample) and ball-milled $Si_{80}Ge_{20}B_{0.6}$ + 0.5vol% SiC composite ($Si_{80}Ge_{20}B_{0.6}$ + 0.5vol% SiC BM sample) before SPS. All the diffraction patterns of these samples match well with those of $Si_{80}Ge_{20}$ alloys[12]. No diffraction peaks of SiC are detected in the $Si_{80}Ge_{20}B_{0.6}$ + 0.5vol% SiC BM sample owing to its low content. The broadened diffraction peaks of the ball-milled samples indicate that the crystallite size of the particles becomes small after ball milling process. The insert in Fig. 1 depicts the XRD pattern of sintered $Si_{80}Ge_{20}B_{0.6}$ + 0.5vol% SiC BM bulk sample. It confirms that the sample maintains a single phase of $Si_{80}Ge_{20}$ alloys after SPS process.

SEM images of commercially available SiC particles with an average particle size about 50 nm, the powders of $Si_{80}Ge_{20}B_{0.6}$ matrix, $Si_{80}Ge_{20}B_{0.6}$ BM and $Si_{80}Ge_{20}B_{0.6}$ + 0.5vol% SiC BM samples are shown in Fig. 2. The mean size of ball-milled $Si_{80}Ge_{20}B_{0.6}$ and ball-milled $Si_{80}Ge_{20}B_{0.6}$ + 0.5vol% SiC composite powders is around 200 nm (Fig. 2(c) and 2(d)) owing to the ball milling process, while the $Si_{80}Ge_{20}B_{0.6}$ matrix particles range in micro scale (Fig. 2b). As a result, as shown in Fig. 3, the sintered samples of $Si_{80}Ge_{20}B_{0.6}$ matrix, $Si_{80}Ge_{20}B_{0.6}$ BM and $Si_{80}Ge_{20}B_{0.6}$+0.5vol% SiC BM keep micro, nano and nano scale, respectively, even though the grain grows slightly during the SPS process. All samples possess clean grain boundaries, which are beneficial to electron transport.

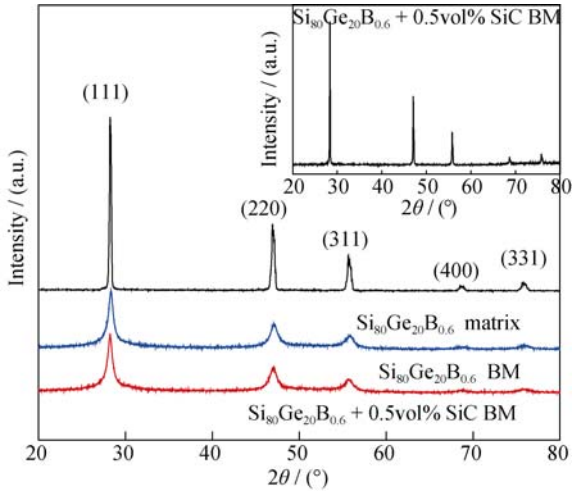

Fig. 1　Powder XRD patterns of $Si_{80}Ge_{20}B_{0.6}$ matrix, $Si_{80}Ge_{20}B_{0.6}$ BM and $Si_{80}Ge_{20}B_{0.6}$ + 0.5vol% SiC BM samples before SPS. The inset in the upper right depicts XRD pattern of $Si_{80}Ge_{20}B_{0.6}$ + 0.5vol% SiC BM sample sintered by SPS

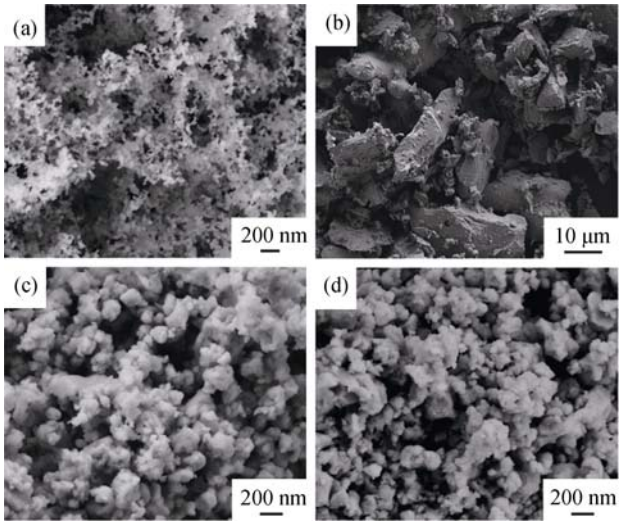

Fig. 2　SEM images of powders before SPS
(a) SiC particles; (b) $Si_{80}Ge_{20}B_{0.6}$ matrix; (c) $Si_{80}Ge_{20}B_{0.6}$ BM, (d) $Si_{80}Ge_{20}B_{0.6}$ + 0.5vol% SiC BM

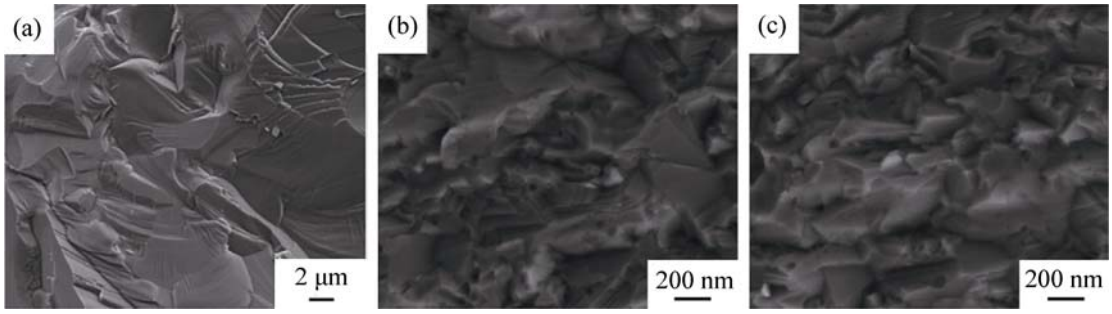

Fig. 3　SEM images of fracture surfaces of bulk samples sintered by SPS
(a) $Si_{80}Ge_{20}B_{0.6}$ matrix; (b) $Si_{80}Ge_{20}B_{0.6}$ BM; (c) $Si_{80}Ge_{20}B_{0.6}$ + 0.5vol% SiC BM

TEM and EDS experiments were conducted to confirm the existence of embedded SiC nanoparticles in the composite samples. Fig. 4 shows TEM images and EDS results of $Si_{80}Ge_{20}B_{0.6}$ + 0.5vol% SiC BM sample. As shown in Fig. 4(a) and 4(c), some nanoparticles with diameters ranging from several tens to two hundred nanometers are observed both at grain boundaries and inside grains in composite sample. Fig. 4(b) is the EDS data of area I and II in Fig. 4(a). EDS result taken around the area I indicates that the chemical composition of the large grain is $Si_{80}Ge_{20}$ alloy, while that of the area II is $Si_{80}Ge_{20}$ and some kind of carbide. A high-resolution TEM (HRTEM) image of the interface between the $Si_{80}Ge_{20}B_{0.6}$ matrix and the embedded nano-carbide is shown in Fig. 4(d). The interface is found to be quite clean and even coherent in some places. In order to exactly confirm the phase composition of nano-carbide, we further analyze the HRTEM images of $Si_{80}Ge_{20}B_{0.6}$ matrix and the carbide nano-grain (Fig. 4(e) and 4(f)). The interplanar spacings of the matrix and carbide nano-grain are 0.316 nm and 0.252 nm, respectively, which accord with that of (111) of cubic $Si_{80}Ge_{20}$ alloy and (111) of cubic SiC, respectively. Moreover, the Fourier transfer diffraction patterns of Fig. 4(e) and 4(f) are given in Fig. 4(g) and 4(h). The diffraction patterns actually conform to that of the cubic $Si_{80}Ge_{20}$ alloy and SiC, respectively, which further indicates the existence of SiC nano-grain being embedded in the $Si_{80}Ge_{20}B_{0.6}$ matrix.

Fig. 5 presents the temperature dependence of electrical conductivity, Seebeck coefficient, power factor (PF = $\alpha^2\sigma$) and carrier concentration for samples of $Si_{80}Ge_{20}B_{0.6}$ matrix, $Si_{80}Ge_{20}B_{0.6}$ BM and $Si_{80}Ge_{20}B_{0.6}$ + $x$vol% SiC BM (x = 0.3, 0.5, 1.0). The electrical conductivity of all samples decreases with temperature, which is consistent with heavily doped semiconducting behavior. The conductivity values of the $Si_{80}Ge_{20}B_{0.6}$ BM and $Si_{80}Ge_{20}B_{0.6}$ + $x$vol% SiC BM samples are much lower than that of the $Si_{80}Ge_{20}B_{0.6}$ matrix sample because of the fine microstructure after ball milling process. Furthermore, the conductivity values of nanocomposite samples decrease slightly with increasing SiC content probably due to the carrier scattering by the SiC nanoparticles. As shown in Fig. 5(b), the Seebeck coefficient values of all ball-milled samples are enhanced significantly in comparison to the matrix sample, and increase slightly with increasing SiC content. The power factor of these ball-milled samples is close to each other, but decreases remarkably in comparison with matrix due

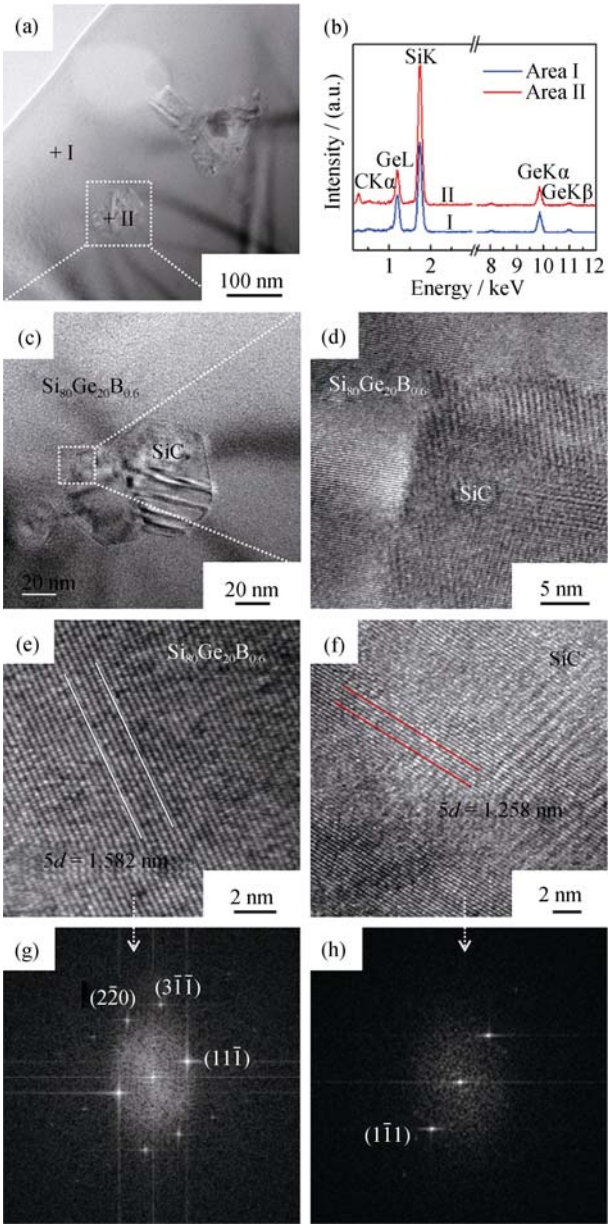

Fig. 4 TEM images and EDS results of $Si_{80}Ge_{20}B_{0.6}$ + 0.5vol% SiC BM sample

(a) TEM image of the composite containing nano-SiC; (b) EDS of the region at areas I and II in (a); (c) High magnification of the sub-region in (a); (d) HRTEM image of the interface between $Si_{80}Ge_{20}B_{0.6}$ matrix and nano-SiC particle; (e, f) HRTEM images of $Si_{80}Ge_{20}B_{0.6}$ matrix and nano-SiC particle, respectively; (g, h) Fourier transfer diffraction patterns of (e) and (f), respectively

to the change in grain size. It is found that carrier concentrations of the $Si_{80}Ge_{20}B_{0.6}$ BM and $Si_{80}Ge_{20}B_{0.6}$ + *x*vol% SiC BM (*x* = 0.3, 0.5, 1.0) samples are essentially identical and decrease on some degree as compared with that of the $Si_{80}Ge_{20}B_{0.6}$ matrix, as shown in Fig. 5(d). This is an authentic evidence that SiC does not change doping content of B and exists as just a second phase. Moreover, such a reduction in carrier concentration after ball milling may ascribed to the oxidation of B element introduced by residual oxygen in the jar during ball milling process. Table 1 presents the room temperature carrier concentration and mobility for all samples calculated from the electrical conductivity and Hall resistance. The carrier mobility of all ball-milled samples is much lower than that of the

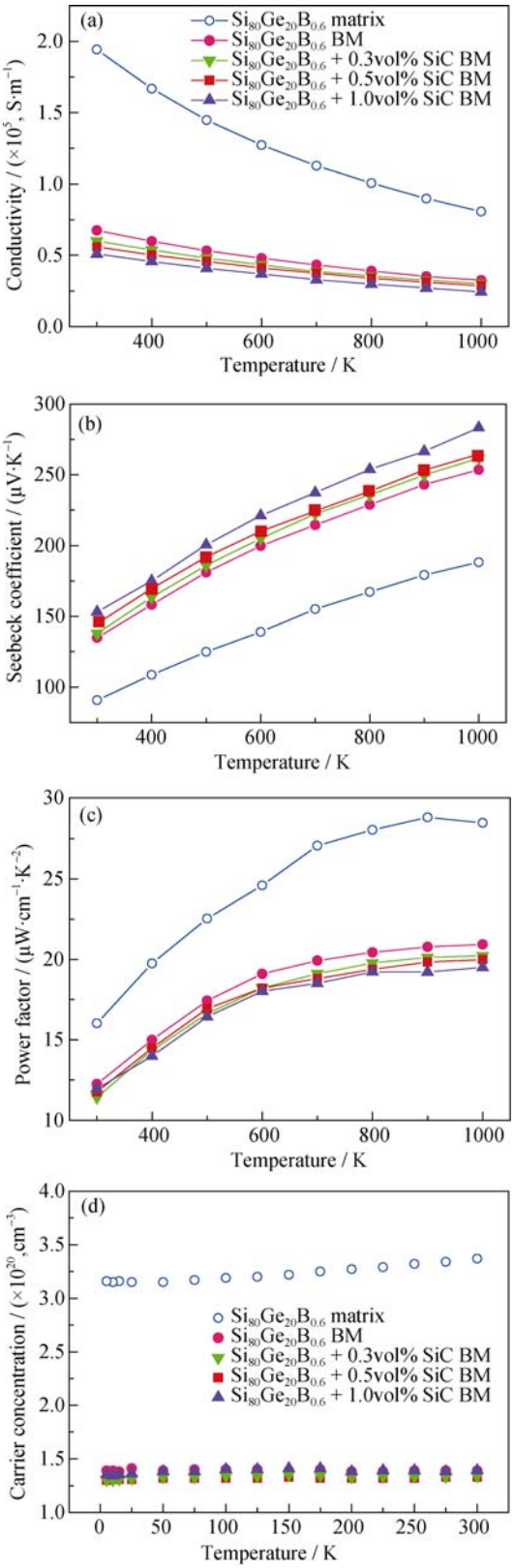

Fig. 5 Temperature dependence of (a) electrical conductivity, (b) Seebeck coefficient, (c) power factor and (d) carrier concentration for $Si_{80}Ge_{20}B_{0.6}$ matrix, $Si_{80}Ge_{20}B_{0.6}$ BM and $Si_{80}Ge_{20}B_{0.6}$ + *x*vol% SiC BM (*x* = 0.3, 0.5, 1.0) samples

Table 1　Room temperature carrier concentration and mobility for $Si_{80}Ge_{20}B_{0.6}$ matrix, $Si_{80}Ge_{20}B_{0.6}$ BM and $Si_{80}Ge_{20}B_{0.6}$ + *x*vol% SiC BM (*x* = 0.3, 0.5, 1.0) samples

Sample	Carrier concentration/ ($\times10^{20}$, cm^{-3})	Carrier mobility/ ($cm^2 \cdot V^{-1} \cdot s^{-1}$)
$Si_{80}Ge_{20}B_{0.6}$ matrix	3.4	36
$Si_{80}Ge_{20}B_{0.6}$ BM	1.4	30
$Si_{80}Ge_{20}B_{0.6}$ + 0.3vol% SiC BM	1.3	28
$Si_{80}Ge_{20}B_{0.6}$ + 0.5vol% SiC BM	1.3	26
$Si_{80}Ge_{20}B_{0.6}$ + 1.0vol% SiC BM	1.4	23

$Si_{80}Ge_{20}B_{0.6}$ matrix sample, which suggests that the carrier scattering introduced by fine microstructure after ball milling process is inevitable. The observed carrier mobility in nanocomposites decreases gradually with increasing SiC content probably due to the enhanced scattering by SiC nanoparticles.

The temperature dependence of the thermal conductivity and lattice thermal conductivity for all samples is plotted in Fig. 6. The thermal conductivity of all samples decreases with increasing temperature over the measured range up to 1000 K. A dramatic reduction in the thermal conductivity is achieved by reducing grain size of $Si_{80}Ge_{20}B_{0.6}$ based on the fact that the ball-milled samples possess lower thermal conductivity than the $Si_{80}Ge_{20}B_{0.6}$ matrix sample. Moreover, the thermal conductivity of composite samples first decreases and then increases with increasing SiC content. Thermal conductivity can be expressed by the sum of lattice thermal conductivity (κ_l) and electronic thermal conductivity (κ_e). The κ_e can be estimated from Wiedemann-Franz's law as $\kappa_e = L_0 T\sigma$, with a Lorenz number L_0 of 2.45×10^{-8} (V^2/K^2), which applies to degenerated semiconductors. Therefore, the lattice thermal conductivity is deduced from the relation $\kappa_l = \kappa - \kappa_e$. As shown in Fig. 6(b), the $Si_{80}Ge_{20}B_{0.6}$ + 0.5vol% SiC BM sample has the lowest lattice thermal conductivity, reaching 2.54 W/(m·K) at 1000 K which is 25% and 10% lower than the matrix sample and $Si_{80}Ge_{20}B_{0.6}$ BM sample, respectively. A more pronounced grain boundary scattering of phonons in the ball-milled samples decreases their lattice thermal conductivity. Furthermore, embedded SiC nanoparticles provide more scattering centers and are indeed effective in scattering phonon. In addition, when the content of SiC reaches 1vol%, slight rising in lattice thermal conductivity appears because of the volume effect of high thermal conductivity of SiC.

The *ZT* values of all samples are shown in Fig. 7. The maximum *ZT* value of $Si_{80}Ge_{20}B_{0.6}$ BM sample with nanostructure is about 0.58 at 1000 K, which is 9% improved as comparison with $Si_{80}Ge_{20}B_{0.6}$ matrix. This increase of *ZT* is thought to majorly result from the decrease in the thermal conductivity due to the enforced phonon scattering by the numerous interfaces. Meanwhile, the presence of 0.5 vol% nano-SiC second phase leads to a higher *ZT* of ~0.62 at 1000 K because of the synergetic effect of nanostructure and nanocomposite. This is about 7%, 17% and 30% higher in comparison to the $Si_{80}Ge_{20}B_{0.6}$ BM sample, $Si_{80}Ge_{20}B_{0.6}$ matrix sample and p-type RTG SiGe alloy used in space flight missions[4], respectively.

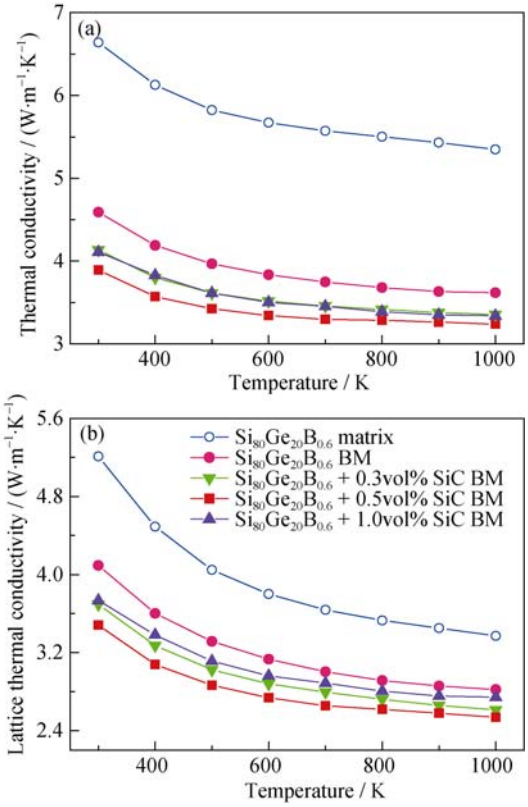

Fig. 6　Temperature dependence of (a) thermal conductivity and (b) lattice thermal conductivity for $Si_{80}Ge_{20}B_{0.6}$ matrix, $Si_{80}Ge_{20}B_{0.6}$ BM and $Si_{80}Ge_{20}B_{0.6}$ + *x*vol% SiC BM (*x* = 0.3, 0.5, 1.0) samples

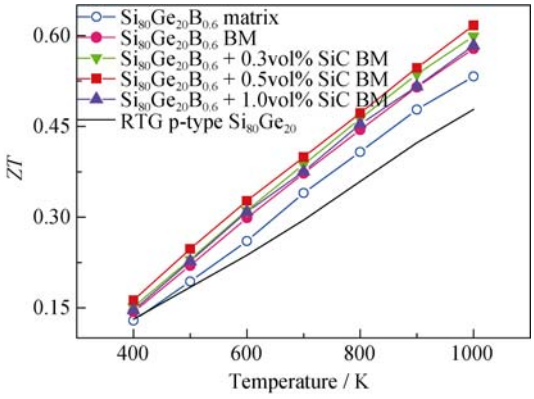

Fig. 7　Temperature dependence of *ZT* values for RTG p-type $Si_{80}Ge_{20}$ alloy[3], $Si_{80}Ge_{20}B_{0.6}$ matrix, $Si_{80}Ge_{20}B_{0.6}$ BM and $Si_{80}Ge_{20}B_{0.6}$ + *x*vol% SiC BM (*x* = 0.3, 0.5, 1.0) samples

3 Conclusions

In summary, $Si_{80}Ge_{20}B_{0.6}$ BM sample and $Si_{80}Ge_{20}B_{0.6}$ + *x*vol% SiC BM (*x* = 0.3, 0.5, 1.0) nanocomposites were synthesized by induction melting, ball milling followed by spark plasma sintering process. The nanocomposites have an average grain size of ~500 nm and contain a certain amount of evenly distributed SiC particles with an average diameter of ~100 nm. The grain size reduction resulting from ball milling as well as the presence of SiC nanoparticles is responsible for the remarkable reduction in lattice thermal conductivity, giving rise to the enhanced *ZT* values in p-type $Si_{80}Ge_{20}B_{0.6}$ alloys. Moreover, nanostructuring and nanocomposite approaches have similar impact when it comes to their contributions to the improvement of TE performance. Furthermore, it is demonstrated that the nanostructuring and nanocomposite can be employed simultaneously to achieve duplicate effect on thermal conductivity reduction for enhancing thermoelectric performance of bulk materials.

References:

[1] SLACK G A, HUSSAIN M A. The maximum possible conversion efficiency of silicon-germanium thermoelectric generators. *Journal of Applied Physics*, 1991, **70(5):** 2694–2718.

[2] STEELE M C, ROSI F D. Thermal conductivity and thermoelectric power of germanium-silicon alloys. *Journal of Applied Physics*, 1958, **29(11):** 1517–1520.

[3] VINING C B. A model for the high-temperature transport-properties of heavily doped n-type silicon-germanium alloys. *Journal of Applied Physics*, 1991, **69(1):** 331–341.

[4] ROWE D M, ed. CRC Handbook of Thermoelectrics. Boca Raton: CRC Press, 1995, chap. 28.

[5] VINING C B, LASKOW W, HANSON J O, *et al*. Thermoelectric properties of pressure-sintered $Si_{0.8}Ge_{0.2}$ thermoelectric alloys. *Journal of Applied Physics*, 1991, **69(8):** 4333–4340.

[6] KUNDU A, MINGO N, BROIDO D A, *et al*. Role of light and heavy embedded nanoparticles on the thermal conductivity of SiGe alloys. *Physical Review B*, 2011, **84(12):** 125426–1–5.

[7] ROWE D M, SHUKLA V S, SAVVIDES N. Phonon scattering at grain boundaries in heavily doped fine-grained silicon-germanium alloys. *Nature*, 1981, **290:** 765–766.

[8] SHI L H, JIANG J J, ZHANG G, *et al*. High thermoelectric figure of merit in silicon-germanium superlattice structured nanowires. *Applied Physics Letters*, 2012, **101(23):** 233114/1–233114/4.

[9] LU J B, GUO R Q, DAI W J, *et al*. Enhanced in-plane thermoelectric figure of merit in p-type SiGe thin films by nanograin boundaries. *Nanoscale*, 2015, **7:** 7331–7339.

[10] MINNICH A J, DRESSELHAUS M S, REN Z F, *et al*. Bulk nanostructured thermoelectric materials: current research and future prospects. *Energy & Environmental Science*, 2009, **2:** 466–479.

[11] DRESSELHAUS M S, CHEN G, TANG M Y, *et al*. New directions for low dimensional thermoelectric materials. *Advanced Materials*, 2007, **19(8):** 1043-1053.

[12] JOSHI G, LEE H, LAN Y C, *et al*. Enhanced thermoelectric figure-of-merit in nanostructured p-type silicon germanium bulk alloys. *Nano Letters*, 2008, **8(12):** 4670–4674.

[13] WANG X W, LEE H, LN Y C, *et al*. Enhanced thermoelectric figure of merit in nanostructured n-type silicon germanium bulk alloy. *Journal of Applied Physics*, 2008, **93(19):** 193121–1–3.

[14] BASU R, BHATTACHARYA S, BHATT R, *et al*. Improved thermoelectric performance of hot pressed nanostructured n-type SiGe bulk alloys. *Journal of Materials Chemistry A*, 2014, **2(19):** 6922–6930.

[15] BATHULA S, JAYASIMHADRI M, GAHTORI B, *et al*. The role of nanoscale defect features in enhancing the thermoelectric performance of p-type nanostructured SiGe alloys. *Nanoscale*, 2015, **7(29):** 12474–12483.

[16] BATHULA S, JAYASIMHADRI M, SINGH N, *et al*. Enhanced thermoelectric figure-of-merit in spark plasma sintered nanostructured n-type SiGe alloys. *Applied Physics Letters*, 2012, **101(21):** 213902/1–213902/5.

[17] POUDEL B, HAO Q, MA Y, LAN Y, *et al*. High-thermoelectric performance of nanostructured bismuth antimony telluride bulk alloys. *Science*, 2008, **320(5876):** 634–638.

[18] ZHOU X, WANG G, ZHANG L, *et al*. Enhanced thermoelectric properties of Ba-filled skutterudites by grain size reduction and Ag nanoparticle inclusion. *Journal of Materials Chemistry*, 2012, **22:** 2958–2964.

[19] ZHAO X Y, SHI X, CHEN L D, *et al*. Synthesis of $Yb_yCo_4Sb_{12}/Yb_2O_3$ composites and their thermoelectric properties. *Applied Physics Letters*, 2006, **89(9):** 092121–1–3.

[20] DING J, LIU R H, GU H, *et al*. Study on the high temperature stability of $Yb_yCo_4Sb_{12}/Yb_2O_3$ composite thermoelectric material. *Journal of Inorganic Materials*, 2014, **29(2):** 209–214.

[21] LI J, TAN Q, LI J, *et al*. BiSbTe-based nanocomposites with high *ZT*: the effect of SiC nanodispersion on thermoelectric properties. *Advanced Functional Materials*, 2013, **23(35):** 4317–4323.

[22] MINGO N, HAUSER D, KOBAYASHI NP, *et al*. "Nanoparticle-in-Alloy" approach to efficient thermoelectrics: silicides in SiGe. *Nano Letters*, 2009, **9(2):** 711–715.

[23] FAVIER K, BERNARD-GRANGER G, NAVONE C, *et al*. Influence of *in situ* formed $MoSi_2$ inclusions on the thermoelectrical properties of an N-type silicon-germanium alloy. *Acta Material*, 2014, **64:** 429–442.

P 型 $Si_{80}Ge_{20}B_{0.6}$-SiC 纳米复合材料的微观结构与热电性能研究

杨小燕[1,3], 吴洁华[2], 任都迪[2], 张天松[2], 陈立东[1]

(1. 中国科学院 上海硅酸盐研究所, 高性能陶瓷和超微结构国家重点实验室, 上海 200050; 2. 中国科学院 上海硅酸盐研究所, 能量转换材料重点实验室, 上海 200050; 3. 中国科学院大学, 北京 100049)

摘 要: 采用感应熔炼、球磨与放电等离子烧结的方法制备了 SiC 第二相均匀分布的 $Si_{80}Ge_{20}B_{0.6}$-SiC 纳米复合热电材料。系统研究了细化 $Si_{80}Ge_{20}B_{0.6}$ 晶粒尺寸与复合 SiC 纳米颗粒对材料热电性能的影响。球磨导致的 $Si_{80}Ge_{20}B_{0.6}$ 晶粒尺寸的降低显著增加了材料的晶界数量, 进而增强了晶界对中长波声子的散射, 能够有效降低材料的晶格热导。$Si_{80}Ge_{20}B_{0.6}$ 基体中均匀分布的纳米 SiC 颗粒提供了额外的散射中心和界面，可进一步增强声子散射，降低材料的晶格热导。在纳米结构化与 SiC 纳米复合的共同作用下, 材料在 1000 K 时热电优值 *ZT* 达到了 0.62, 较基体提高了 17%。证明纳米结构化与纳米复合方法能够共同作用于硅锗合金, 提高其热电性能。

关　键　词: 硅锗合金; SiC 纳米颗粒; 热电材料; 纳米复合; 纳米结构

中图分类号: TQ174　　**文献标识码:** A